Study of Composition Variation on Dielectric and Impedance Spectra of Tetragonal-Rhombohedral System in (1-*x*)BZT-(*x*)BCT Composites

Himani[1], Shweta Thakur[2], Anupinder Singh[3] and Radheshyam Rai[3,4,*]

[1]*Department of Physics, ACBS, Eternal University, Baru Sahib 173101, Himachal Pradesh, India*

[2]*Department of Physics, School of Basic and Applied Sciences, Lingaya's Vidyapeeth, Faridabad, India*

[3]*Multifunctional Materials Laboratory, Department of Physics, Guru Nanak Dev University, Amritsar, Punjab, India-143005*

[4]*School of Physics and Materials Science,Shoolini University, Solan-173229 HP*

Abstract: In present work, (1-*x*)[$BaZr_{0.2}Ti_{0.8}O_3$]-(*x*)[$Ba_{0.7}Ca_{0.3}TiO_3$] (BZT-BCT) (where *x* = 0.50, 0.60 and 0.75) were fabricated by solid-state reaction technique. Structural, dielectric and impedance properties of the synthesized composites were investigated and discussed in detail. The X-ray diffraction technique shows that all the samples possessed a double-phase polycrystalline sample with a tetragonal-rhombohedral structure. Dielectric and impedance behavior were investigated in a wide range of temperatures (room temperature (RT) - 500˚C) and frequency (100 Hz ≤f ≤ 1 MHz). A broad dielectric constant peak was observed around the phase transition temperature.

Keywords: Structural, Dielectric, Impedance, Ferroelectric, BZT.

INTRODUCTION

Lead-based piezoelectric ceramics have PZT that has widely used as sensors, actuators, transformers and in other ferroelectric devices due to its piezoelectric-ferroelectric properties [1-4]. However, lead-based PZT materials contain more than 60 wt.% of lead oxide which causes various environmental problems and numerous medical diseases symptoms like headaches, constipation, nausea, anemia, nerve, brain and kidney damage, etc. [5]. WEEE (Waste Electrical and Electronic Equipment) and RoHS (Restriction of Dangerous Substances) have placed a ban on the use of lead-based materials due to various increased awareness of environmental concerns [6]. Research now based on lead-free functional materials due to recent developments in ecological sensitivity [7-14].

PZT materials, composition showing high electrical and dielectric with Zr/Ti ratio 52/48 properties were close to the morphotropic phase boundary (MPB), where rhombohedral (Zr-rich) and tetragonal (Ti-rich) ferroelectric phase coexistence [15]. But lead-free piezoelectric ceramics is generally inferior piezoelectricity (d_{33} < 150 pC/N compared to d_{33} ~ 500–600 pC/N for lead-based ceramics). Recently. Their range has pushed to a higher level of d_{33} ~ 300 pC/N, but still, it is the most wanted PZT based system [16]. The author reported a lead-free pseudo-binary *x*[$Ba(Zr_{0.2}Ti_{0.8})O_3$ – (1-*x*)[$(Ba_{0.7}Ca_{0.3})TiO_3$] [BZT-BCT], ferroelectric systems to replace PZT based systems. Near this system, MPB was similar to PZT near BZT-BCT (50/50) composition. Piezoelectric, ferroelectric and electromechanical properties for the composition has expected to be the best for this system. They reported that BZT-BCT (50/50) ferroelectric system with surprisingly high piezoelectric properties in this optimal structure [17]. The piezoelectric properties of BZT-*x*BCT systems were particularly affected by temperature, especially piezoelectric properties of compositions that have the largest d_{33} values [18-21]. The BZT-BCT ceramic composites are appropriate for idle applications such as diagnostic instruments in health, sonar devices in the military field, ambient energy harvesting, etc. [22].

It's known that the characteristic piezoelectric and ferroelectric parameters such as d_{33}, polarization (P) and coercive field (E_C) are profoundly affected by several factors such as the distribution of grain size, density, porosity etc. [23].

Lead-free BZT – BCT, solid solutions with high dielectric constant, low loss and high piezoelectric properties with optimum compositions inspired us to use the pseudobinary ferroelectric BZT – BCT solid solution device for dielectric tunable storage capacitor applications. In the present work we, therefore, investigated structural, temperature and frequency-dependent dielectric properties, ferroelectric, ac-conductivity and diffuse phase transition (DPT) behaviour of BZT–BCT ceramics.

Address correspondence to this article at the School of Physics and Materials Science, Shoolini University, Solan, Bajhol, Himachal Pradesh india-173229; Tel: 0091-8521588056;
E-mail: raiphy090116@gmail.com; rshyam1273@gmail.com

E-ISSN: 2409-9848/22

EXPERIMENTAL PROCEDURE

Solid solutions of $\{(x)Ba(Zr_{0.2}Ti_{0.8})O_3 - (1\text{-}x)(Ba_{0.7}Ca_{0.3})TiO_3\}$; ceramics (where x = 0.50, 0.60 and 0.75) (onward "BZT-BCT") were prepared by a solid-state reaction method in the desired stoichiometry. Initially, powders were ball milled for 24 using zirconia balls in the acetone medium. After drying, the powder were calcined at 1200ºC for 12 hrs in a ceramic crucible to for thr phase formation. The calcined powder was pressed into pellets of 1 mm in thickness and 10 mm in diameter using a hydraulic press. The pellets were then sintered at 1250ºC for 2 hr.

An X-Ray Diffraction study has carried out using a PANalytical X'Pert Pro equipped with a CuK_α anode (λ = 1.5406 Å). XRD data were collected from 20º to 80º at a step size 0.01º and a scan speed of 2º/min. In order to analyze the electrical characterization, the upper and lower surfaces of sintered pellets were coated with silver paste (as electrodes) and dried in the air for 1 hr before carrying out the measurements. The electrical parameters were calculated using an impedance analyzer (Keysight-E4990A) in conjunction with a laboratory-constructed sample holder over a temperature range of 410ºC-500ºC and at a frequency of 100Hz-1MHz.

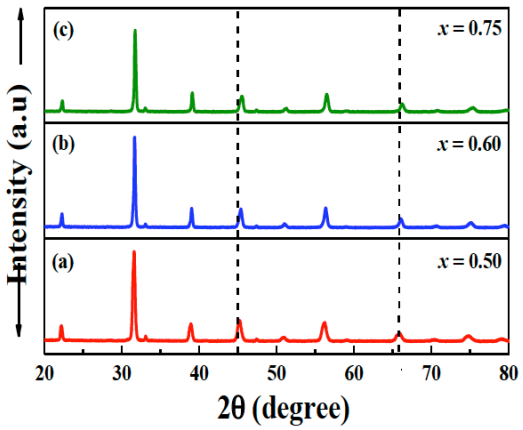

Figure1: X-ray diffraction of $(1\text{-}x)BaZr_{0.2}Ti_{0.8}O_3$ - $(x)Ba_{0.7}Ca_{0.3}TiO_3$ ceramics for compositions (**a**) x = 0.50, (**b**) x = 0.60 and (**c**) x = 0.75.

RESULTS AND DISCUSSION

Structural Properties

Figure **1** shows x-ray diffraction (XRD) patterns obtained at room temperature for sintered samples of various compositions of $\{(x)Ba(Zr_{0.2}Ti_{0.8})O_3\text{-}(1\text{-}x)(Ba_{0.7}Ca_{0.3})TiO_3\}$, (where x = 0.50, 0.60 and 0.75). All the compositions exhibit

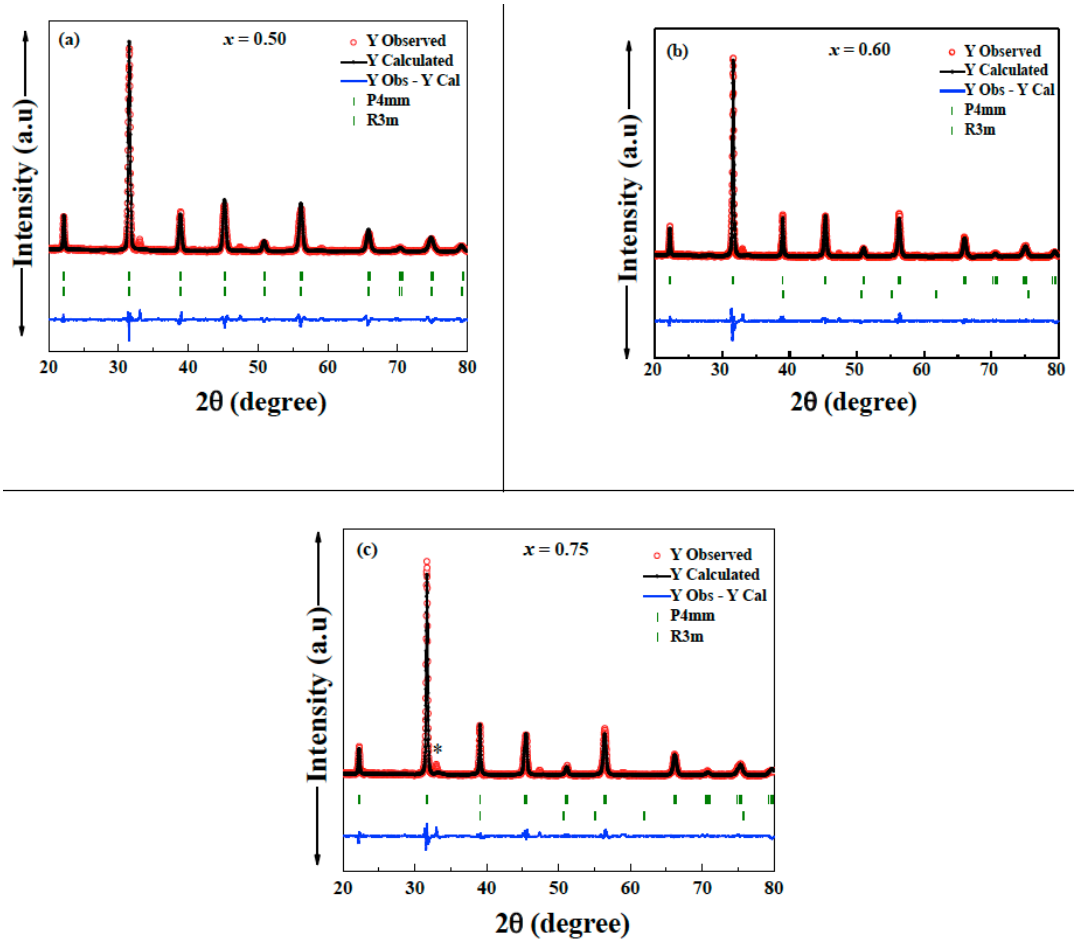

Figure 2(a-c): Observed and Calculated XRD pattern of $(1\text{-}x)BaZr_{0.2}Ti_{0.8}O_3$ - $(x)Ba_{0.7}Ca_{0.3}TiO_3$ ceramics for compositions (**a**) x = 0.50, (**b**) x = 0.60 and (**c**) x = 0.75.

double-phase formation. The reflections in the XRD patterns are indexed using P4mm space group symmetry with a tetragonal structure and R3m space group symmetry with a rhombohedral structure. The position of the diffraction peaks gradually shift towards higher diffraction angles with increases in the BCT content. The shifting of peaks indicates that the interplanar spacing decreases with increases in the BCT content. This decrease in the lattice parameters could be attributed to the substitution of ions with different ionic radii at the A-site and B-site of BZT-BCT, such as Ba^{2+} (1.61 Å), Zr^{4+} (0.72 Å), Ca^{2+} (1.34 Å) and Ti^{4+} (0.605 Å). The characteristic is by splitting of (002)/(200) peaks at around 2θ ~ 45º and as well as the splitting of the (202)/(220) peaks at around 2θ ~ 65º- 66º [24-31]. Peaks splitting at both 2θ ~ 45º and 2θ ~ 65º-66º confirms both tetragonal and rhombohedral phase coexistence in BZT-BCT ceramics. XRD patterns for all the prepared samples were refined by using Rietveld analysis. The occupancy parameters fixed according to the stoichiometric composition. The lattice parameters, z-position coordinates and isotropic thermal parameters were refined for the phase as well. A Pseudo-Voigt function has used to describe peak profile and linear interpolation between a set background points with refinable heights. The various refinable parameters sequentially refined until the minimum values of G.O.F. and other discrepancy parameters obtained. The Rietveld refined data for all the samples are shown in Figure **2(a-c)**. The data clearly show a very good agreement between the experimental and theoretically simulated data. The final values of various refined parameters have listed in Table **1**. The variations in the lattice parameters ("a" and "c") and cell volume for multiple compositions, as shown in Figure **3 (a-b)**. It can be observed from the figure that the values for both the lattice parameters "a" and "c" for both the phases decreases with increases in the *x*-variations and lead to a corresponding decrease in the cell volume.

Dielectric Studies

Figure **4(a-c**) shows the temperature dependence of the dielectric constant at various frequencies for sintered BZT-BCT pellets at 1250ºC/2h. The overall dielectric properties of all ceramics are summarized in Table **2**. All samples exhibit a broad dielectric anomaly associated with rhombohederal-tetragonal (R-T) phase transition. This dielectric broadening is due to compositional fluctuations and micro-inhomoginity [32]. Meanwhile, all peak temperatures are dependent on the frequency and shift to high temperature with frequency increasing. In other words, all BZT-BCT ceramics represent a relaxor behavior [33, 34]. Figure **5(a-c)** shows the limiting values γ =1 and γ = 2 reduce the equation to Curie-Weiss law for the case of normal ferroelectric respectively. The effect of

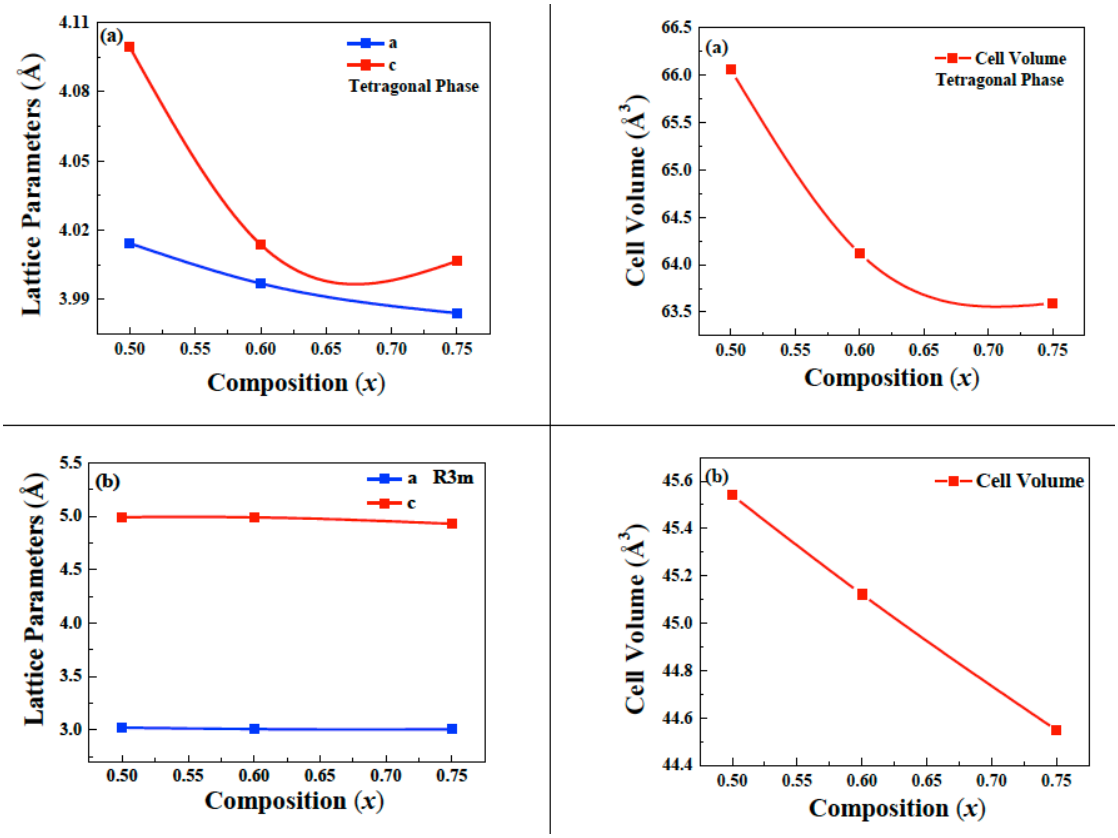

Figure 3 (a-b): Variations in (**a**)-(**b**) is lattice parameters ("a" and "c") and cell volume as functions of the composition (*x*) for (1-*x*)$BaZr_{0.2}Ti_{0.8}O_3$ - (*x*)$Ba_{0.7}Ca_{0.3}TiO_3$ ceramics.

Table 1: FullPROF Based Rietveld Refinement Parameters and Calculated Crystallographic Parameters of the XRD Pattern of (1-*x*)$BaZr_{0.2}Ti_{0.8}O_3$ - (*x*)$Ba_{0.7}Ca_{0.3}TiO_3$ (where *x* = 0.50, 0.60 and 0.75) Ceramics

Calculated Crystallographic Parameters			*x* = 0.50	*x* = 0.60	*x* = 0.75
Lattice Parameters Tetragonal	a = b (Å)		4.0143	3.9969	3.9843
	c (Å)		3.9993	4.0138	4.0063
c/a Ratio of Tetragonal	c/a		0.9962	1.0042	1.0055
Tetragonal phase present (%)			95.71	95.25	61.84
Volume of unit cell Tetragonal	V ($Å^3$)		64.446	64.121	63.600
Lattice Parameters Rhombohedral	a (Å)		3.0201	3.0051	2.9964
	c (Å)		4.9424	4.9914	4.9983
Rhombohedral phase present (%)			4.29	4.75	38.16
Volume of unit cell Rhombohedral	V ($Å^3$)		39.047	39.037	38.865
Atomic Positions	Ba/Ca	X	0	0	0
		Y	0	0	0
		Z	0	0	0
	Zr/Ti	X	0.5	0.5	0.5
		Y	0.5	0.5	0.5
		Z	0.51680	0.50991	0.48481
	O1	X	0.5	0.5	0.5
		Y	0.5	0.5	0.5
		Z	0.04081	0.07311	-0.04089
	O2	X	0.5	0.5	0.5
		Y	0	0	0
		Z	0.53735	0.49769	2.53287
R – Factor (%) Tetragonal	R_p		18.6	17.5	17.8
	R_{wp}		17.4	18.7	19.4
	R_e		9.81	9.57	10.4
	R_f		2.18	1.74	2.76
	R_B		3.40	3.06	4.67
R – Factor (%) Rhombohedral	R_p		……	……	……
	R_{wp}		……	……	……
	R_e		……	……	……
	R_f		9.21	20.1	11.9
	R_B		8.76	18.3	3.92
GOF	χ^2		3.161	3.804	3.462
Experimental Density	δ (g/cm^3)		5.106	5.077	5.028
Crystallite size (nm)	Calculated By W-H Plot		17.295	25.388	23.621
Lattice strain (ε) $\times 10^{-3}$			5.61	3.35	4.73
Bond Angle (θ) for Tetragonal	O_1 – Ba – O_1		89.8112	89.3889	89.8068
	O_2 – Ba – O_2		62.6516	60.0135	90.192
	O_1 – Zr – O_1		180	180	180
	O_2 – Zr – O_2		175.3105	177.1881	172.7
Bond Length (Å) for Tetragonal	O_1 - Ba		2.8432	2.8414	2.8220
	O_2 - Ba		2.7298	2.8256	2.7333
	O_1 - Zr		1.9036	1.7532	1.835
	O_2 - Zr		2.0088	1.9990	1.9962

Bond Angle (θ) for Rhombohedral	$O_1 – Ba – O_1$	34.76	29.992	30.5926
	$O_2 – Ba – O_2$	33.37	40.218	45.3315
	$O_1 – Zr – O_1$	37.88	53.885	35.8641
	$O_2 – Zr – O_2$	61.12	34.700	102.7760
Bond Length (Å) for Rhombohedral	O_1 - Ba	3.1436	3.1283	2.8395
	O_2 - Ba	2.6300	2.1851	1.1798
	O_1 - Zr	2.3263	1.7354	1.9231
	O_2 - Zr	1.8754	2.6394	1.4991

Table 2: Dielectric Parameters of (1-*x*)Ba($Zr_{0.2}Ti_{0.8}$)O_3 – (*x*)($Ba_{0.7}Ca_{0.3}$)TiO_3 Ceramics at *x* = 0.50, 0.60 and 0.75 Compositions

x-variations	T_m (ºC)	ε_{max}	tan δ	T_{cw} (ºC)	T_o	T_o - T_o	γ
0.50	122	1189.37	0.01631	153	127	31	1.09
0.60	138	2310.06	0.33236	159	137	21	1.10
0.75	136	1860.16	0.06624	160	143	24	1.16

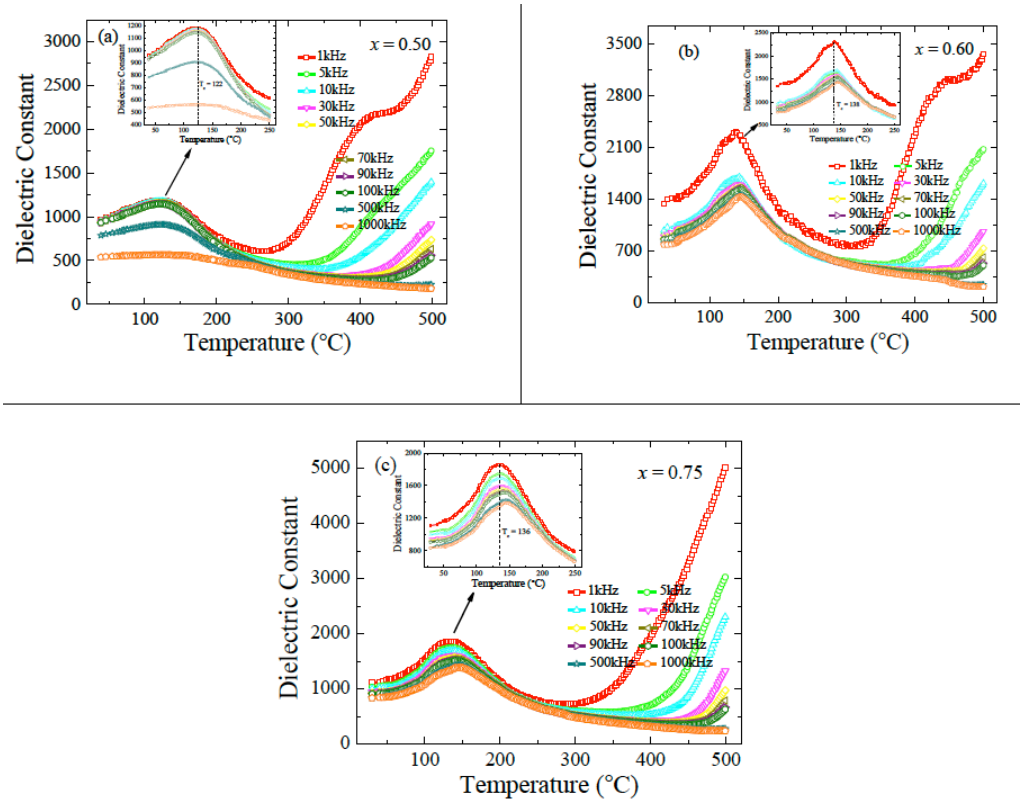

Figure 4(a-c): Temperature dependence of Dielectric constant (ε') for (1-*x*)$BaZr_{0.2}Ti_{0.8}O_3$ - (*x*)$Ba_{0.7}Ca_{0.3}TiO_3$ ceramics for compositions (**a**) *x* = 0.50, (**b**) *x* = 0.60 and (**c**) *x* = 0.75.

temperature on diffuseness γ (diffusivity) from slope of $\ln(1/\varepsilon - 1/\varepsilon_{max})$ vs. $\ln(T - T_{max})$. We obtained the value of the parameters γ is 1.16, 1.10 and 1.09 shown in Table **2** which is between 1 and 2, which suggesting that the samples are relaxor ferroelectrics [35, 36].

Complex Impedance Analysis

The variation of real part Z′ of impedance as a function of frequency (100 Hz – 1 MHz) at different temperatures (410ºC - 500ºC) is shown in Figure **6(a-c)**. It was observed that the magnitude of Z′ is high in the low-frequency region a decrement is observed with increase in frequency, showing a typical negative temperature coefficient of resistance (NTCR) type behaviour [37]. A decrement in Z′ with the rise in temperature and frequency indicates a possibility of an increase in ac conductivity with temperature [38,39]. In the high-frequency region, Z′ merges at all temperatures due to the release of space charge. As a result, the barrier properties in the material reduce [40-43]. The variation of imaginary part (Z″) of

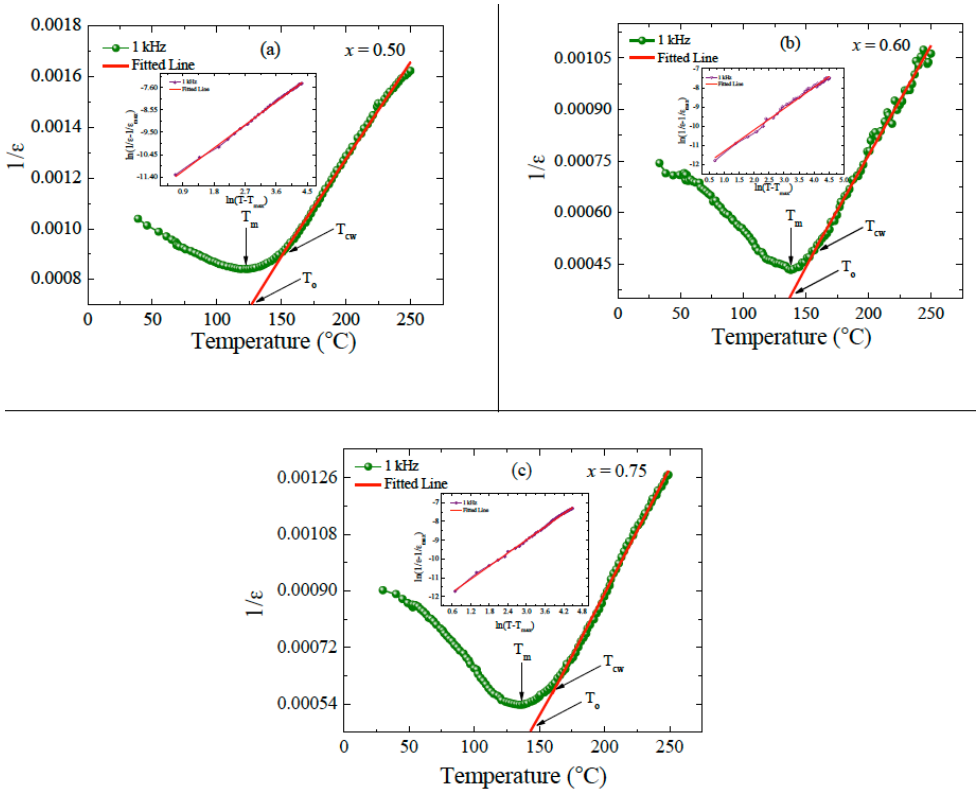

Figure 5(a-c): Temperature dependence of Diffusivity (γ) for (1-x)$BaZr_{0.2}Ti_{0.8}O_3$ - (x)$Ba_{0.7}Ca_{0.3}TiO_3$ ceramics for compositions (**a**) x = 0.50, (**b**) x = 0.60 and (**c**) x = 0.75.

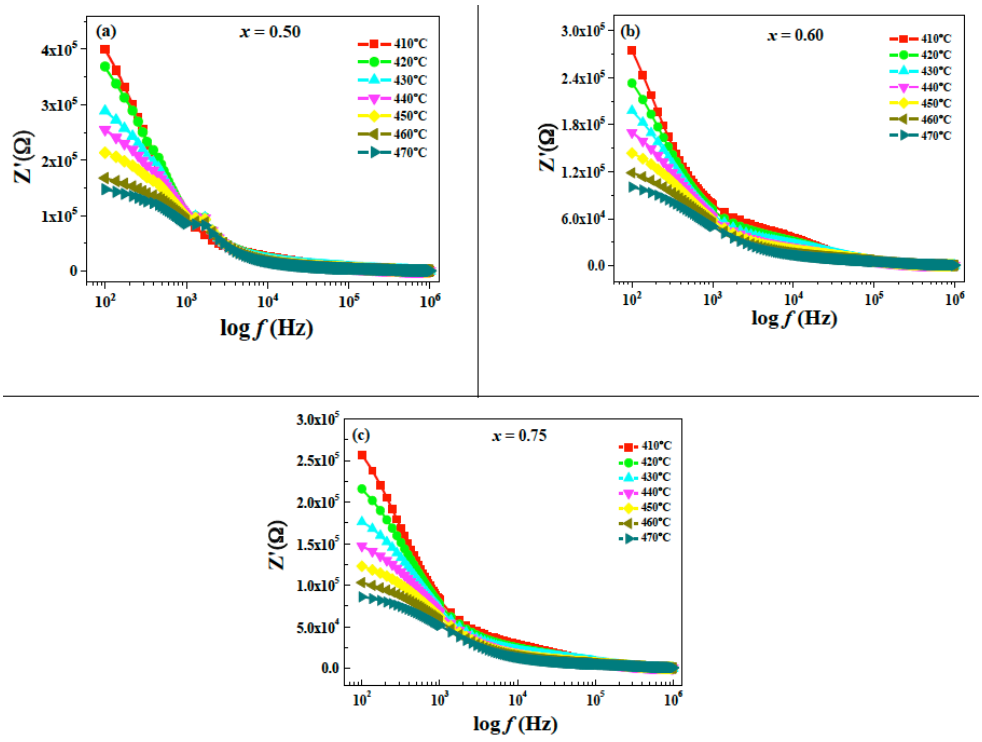

Figure 6(a-c): Frequency dependence of real part(Z′) of impedance for (1-x)$BaZr_{0.2}Ti_{0.8}O_3$ - (x)$Ba_{0.7}Ca_{0.3}TiO_3$ ceramics for compositions (**a**) x = 0.50, (**b**) x = 0.60 and (**c**) x = 0.75.

impedance as a function of frequency at different temperatures as shown in Figure **7(a-c**). Z″ values decrease with a rise in temperature as well as the frequency, which reveals a reduction in the sample's resistive properties. Z″ values decrease with a rise in temperature as well as the frequency, which reveals a reduction in the sample's resistive properties. The relaxation process may be due to immobile species/electrons at low temperature and defects/vacancies at a higher temperature [37-38,44]. Furthermore, a higher frequency may be due to the disappearance of space charge polarization [**b**].

Table 3: The Grain and Grain Boundary Contributions Evaluated after Fitting of impedance data for *x* 0.50, 0.60 and 0.75 Samples

	x = 0.50				*x* = 0.60				*x* = 0.75			
Temp (ºC)	R_g (Ω)	C_g (nF)	R_{gb} Ω)	C_{gb} (nF)	R_g (Ω)	C_g (nF)	R_{gb} (Ω)	C_{gb} (nF)	R_g (Ω)	C_g (nF)	R_{gb} (Ω)	C_{gb} (nF)
410	14534	0.1662e-9	510697	1.184e-9	335898	2.48e-9	39345	0.1722e-9	293812	1.637e-9	19889	0.1303e-9
420	10653	0.1528e-9	436325	1.086e-9	259807	2.329e-9	30255	0.1651e-9	244114	1.666e-9	14897	0.1301e-9
430	6949	0.1582e-9	337072	1.078e-9	203312	2.143e-9	23105	0.1568e-9	198508	1.677e-9	11007	0.1281e-9
440	5533	0.1617e-9	287717	1.059e-9	180257	2.249e-9	18365	0.1628e-9	163440	1.676e-9	8133	0.1252e-9
450	3893	0.1695e-9	245316	1.094e-9	153706	2.231e-9	14113	0.1635e-9	134205	1.642e-9	6033	0.1205e-9
460	2797	0.1722e-9	187128	1.058e-9	131705	2.152e-9	7636	0.1553e-9	112009	1.679e-9	4571	0.1193e-9
470	2246	0.1764e-9	162939	1.06e-9	112498	2.218e-9	5398	0.1525e-9	92698	1.684e-9	3546	0.1164e-9

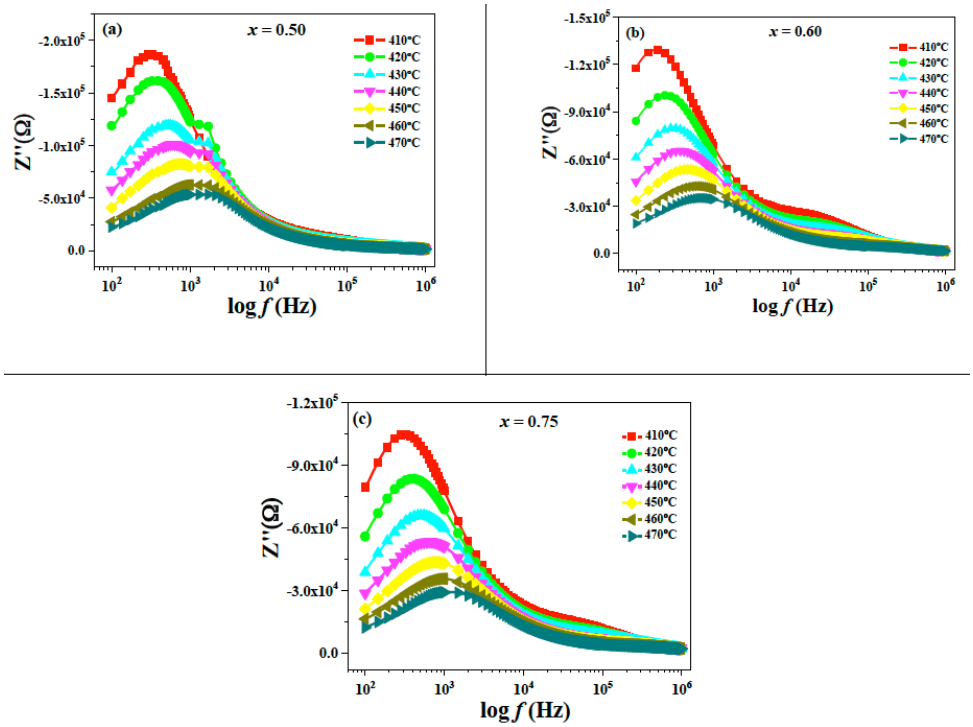

Figure 7(a-c): Frequency dependence of imaginary part(Z″) of impedance for (1-*x*)$BaZr_{0.2}Ti_{0.8}O_3$ - (*x*)$Ba_{0.7}Ca_{0.3}TiO_3$ ceramics for compositions (**a**) *x* = 0.50, (**b**) *x* = 0.60 and (**c**) *x* = 0.75.

Peak position gives the relaxation time according to the relation $2\pi f_{max}\,\tau = 1$, where f_{max} is the frequency at the maximum of Z'' vs. frequency and τ is the relaxation time. From the peak position evaluated the relaxation frequency and time of Z'' with frequency plots at different temperatures. The nature variation of τ^Z as the inverse of absolute temperature is given in Figure **8(a-c)**. The value of activation energy from the slope of linear fit of $\ln(\tau^Z)$ vs. 10^3T^{-1} is 0.9202 eV, 1.0136 eV and 0.9610 eV. Widening of the Z'' with an increase in temperature indicates a non-unique relaxation time scale, whose distribution is wider on the high frequency side after the maximum peak position [47].

To examine the temperature-dependent relaxation time distribution, a normalized plot of Z''/Z''_{max} vs. frequency at different temperatures has been ploted as shown in Figure **9(a-c)**. The imaginary part of impedance collapsed into one master curve shows that the dispensation of relaxation time is temperature independent and dynamic processes of charges that occour on different time scales obtain the identical activation energy. Figure **10(a-c)** shows that the plot of complex impedance spectrum (Nyquist plot) and their fitting results taken over a frequency range ($100\,Hz \leq f \leq 1\,MHz$) at different temperature and frequency has been selected as semicircles appeared in the Nyquist plots within this temperature region. Further, the decrease of radii with rise in temperature manifests the NTCR behavior of the material. To analyze the impedance spectra, data are usually modelled by an ideal equivalent circuit (using EC-fit software) as shown in inset of figure. The complex plane plots two semi-circular arcs well separated at the higher temperature. This behavior could be attributed to

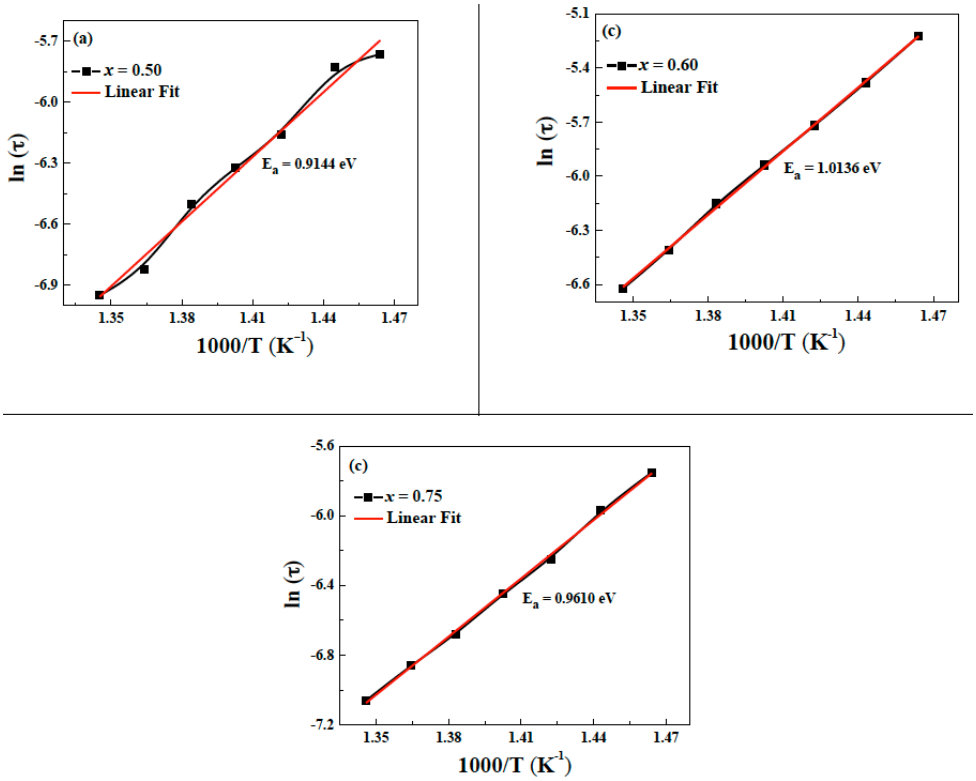

Figure 8(a-c): Arrhenius fit to the relaxation time (τ^Z) imaginary part (Z″) of impedance for (1-*x*)$BaZr_{0.2}Ti_{0.8}O_3$ - (*x*)$Ba_{0.7}Ca_{0.3}TiO_3$ ceramics for compositions (**a**) *x* = 0.50, (**b**) *x* = 0.60 and (**c**) *x* = 0.75.

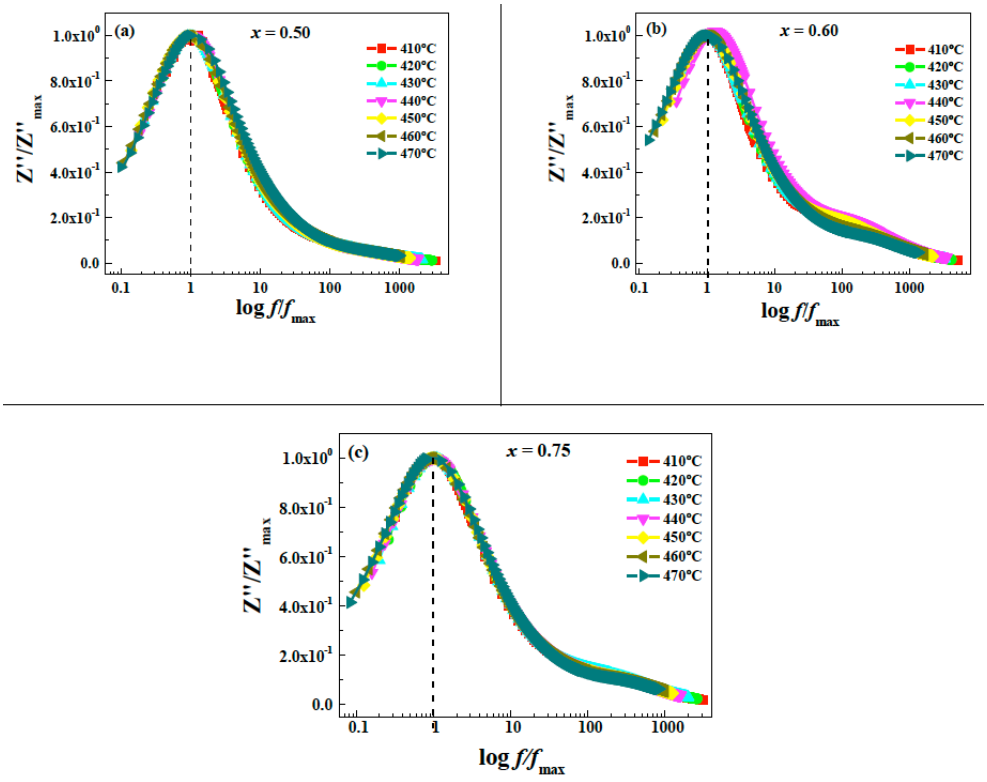

Figure 9(a-c): Normalized plot of imaginary part of impedance (Z'') spectra for (1-*x*)$BaZr_{0.2}Ti_{0.8}O_3$ - (*x*)$Ba_{0.7}Ca_{0.3}TiO_3$ ceramics for compositions (**a**) *x* = 0.50, (**b**) *x* = 0.60 and (**c**) *x* = 0.75.

several factors such as grain orientation, grain boundary, stress-strain phenomena and atomic defect distribution [**37**] where conduction through grain and grain boundaries dominates [38, 48]. The circuit consists of series of two sub circuits, indicating grain and grain boundary contributions. The grain circuit consistes of parallel combination of R_g and CPE_g, whereas the grain boundary consists of parallel combination of R_{gb} and CPE_{gb}.

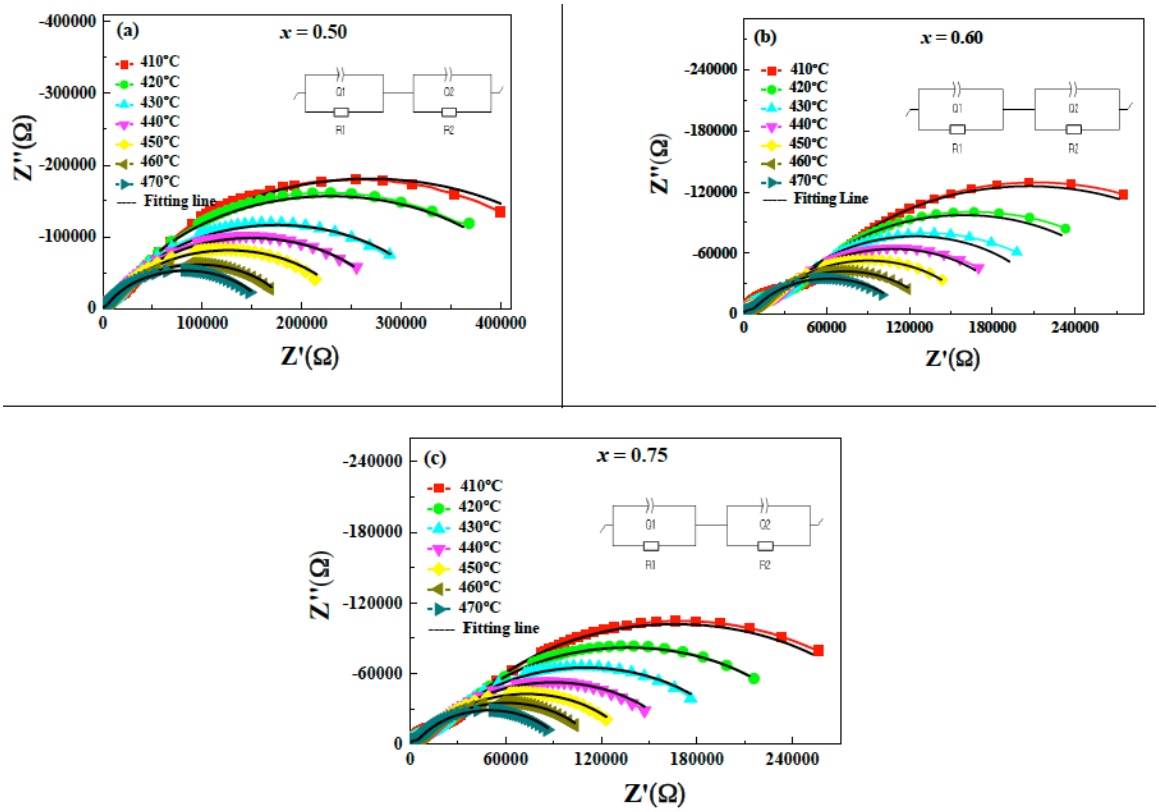

Figure 10(a-c): Nyquist plot of complex impedance (Z′ vs. Z″) at different temperatures for (1-*x*)$BaZr_{0.2}Ti_{0.8}O_3$ - (*x*)$Ba_{0.7}Ca_{0.3}TiO_3$ ceramics for compositions (**a**) *x* = 0.50, (**b**) *x* = 0.60 and (**c**) *x* = 0.75.

CONCLUSION

(1-x)[$BaZr_{0.2}Ti_{0.8}O_3$]-(x)[$Ba_{0.7}Ca_{0.3}TiO_3$] (where x = 0.50, 0.60 and 0.75 volume fractions) were fabricated by solid-state reaction technique. X-ray diffraction technique shows that all the samples possessed a double-phase polycrystalline sample with a tetragonal-rhombohedral structure. Dielectric and impedance behavior were investigated in a wide range of temperatures (room temperature (RT) - 500˚C) and frequency (100 Hz ≤f ≤ 1 MHz). A broad dielectric constant peak was observed around the phase transition temperature. The Nyquist plots revealed the existence of grain and grain boundaries in the overall impedance.

REFERENCES

[1] Jaffe WR. (1971). Cook, and H. Jaffe, Piezoelectric Ceramics. https://doi.org/10.1016/B978-0-12-379550-2.50015-6

[2] Moulson AJ, Herbert JM, & Ceramics E. (1990). Materials properties and Applications.

[3] Haertling GH. (1999). Ferroelectric ceramics: history and technology. Journal of the American Ceramic Society, 82(4), 797-818. https://doi.org/10.1111/j.1151-2916.1999.tb01840.x

[4] Waanders JW. Piezoelectric Ceramics, Properties & Applications, Philips Components, Eindhoven, 1991. Google Scholar There is no corresponding record for this reference.

[5] Takenaka T, & Nagata H. (2005). Current status and prospects of lead-free piezoelectric ceramics. Journal of the European Ceramic Society, 25(12), 2693-2700. https://doi.org/10.1016/j.jeurceramsoc.2005.03.125

[6] Lee GM. (2004). Agency for Technology and Standards, Industry and Energy of the Korean Government. In Seminar on EU Product-Related Regulations (p. 6).

[7] Shrout TR, & Zhang SJ. (2020). Lead-free piezoelectric ceramics: Alternatives for PZT?. In Progress in Advanced Dielectrics (pp. 295-327). https://doi.org/10.1142/9789811210433_0006

[8] Mishra P, & Kumar P. (2012). Effect of sintering temperature on dielectric, piezoelectric and ferroelectric properties of BZT-BCT 50/50 ceramics. Journal of Alloys and Compounds, 545, 210-215. https://doi.org/10.1016/j.jallcom.2012.08.017

[9] Yoon MS, Khansur NH, Choi BK, Lee YG, & Ur SC. (2009). The effect of nano-sized BNBT on microstructure and dielectric/piezoelectric properties. Ceramics International, 35(8), 3027-3036. https://doi.org/10.1016/j.ceramint.2009.04.016

[10] Wu J, Xiao D, Wu W, Chen Q, Zhu J, Yang Z, & Wang J. (2012). Composition and poling condition-induced electrical behavior of (Ba0. 85Ca0. 15)(Ti1− xZrx) O3 lead-free piezoelectric ceramics. Journal of the European Ceramic Society, 32(4), 891-898. https://doi.org/10.1016/j.jeurceramsoc.2011.11.003

[11] Lin W, Fan L, Lin D, Zheng Q, Fan X, & Sun H. (2013). Phase transition, ferroelectric and piezoelectric properties of $Ba_{1-x}Ca_xTi_{1-}$ $yZryO_3$ lead-free ceramics. Current applied physics.

[12] Wang P, Li Y, & Lu Y. (2011). Enhanced piezoelectric properties of (Ba0. 85Ca0. 15)(Ti0. 9Zr0. 1) O3 lead-free ceramics by optimizing calcination and sintering temperature. Journal of the European Ceramic Society, 31(11), 2005-2012. https://doi.org/10.1016/j.jeurceramsoc.2011.04.023

[13] Rani R, Sharma S, Rai R, & Kholkin AL. (2012). Doping effects of Li-Sb content on the structure and electrical properties of [(Na0. 5K0. 5) 1− x (Li) x (Sb) x (Nb) 1− xO3] lead-free piezoelectric ceramics. Materials Research Bulletin, 47(2), 381-386. https://doi.org/10.1016/j.materresbull.2011.11.003

[14] Chen T, Zhang T, Zhou J, Zhang J, Liu Y, & Wang G. (2012). Ferroelectric and piezoelectric properties of [(Ba1− 3x/2Bix) 0.85 Ca0. 15](Ti0. 90Zr0. 10) O3 lead-free piezoelectric ceramics. Materials Research Bulletin, 47(4), 1104-1106. https://doi.org/10.1016/j.materresbull.2012.01.017

[15] Prabu M, Banu IS, Gobalakrishnan S, & Chavali M. (2013). Electrical and ferroelectric properties of undoped and La-doped PZT (52/48) electroceramics synthesized by sol-gel method. Journal of alloys and compounds, 551, 200-207. https://doi.org/10.1016/j.jallcom.2012.09.095

[16] Mishra P, & Kumar P. (2012). Effect of sintering temperature on dielectric, piezoelectric and ferroelectric properties of BZT-BCT 50/50 ceramics. Journal of Alloys and Compounds, 545, 210-215. https://doi.org/10.1016/j.jallcom.2012.08.017

[17] Liu W, & Ren X. (2009). Large piezoelectric effect in Pb-free ceramics. Physical review letters, 103(25), 257602. https://doi.org/10.1103/PhysRevLett.103.257602

[18] Bao H, Zhou C, Xue D, Gao J, & Ren X. (2010). A modified lead-free piezoelectric BZT-xBCT system with higher TC. Journal of Physics D: Applied Physics, 43(46), 465401. https://doi.org/10.1088/0022-3727/43/46/465401

[19] Su S, Zuo R, Lu S, Xu Z, Wang X, & Li L. (2011). Poling dependence and stability of piezoelectric properties of Ba (Zr0. 2Ti0. 8) O3-(Ba0. 7Ca0. 3) TiO3 ceramics with huge piezoelectric coefficients. Current Applied Physics, 11(3), S120-S123. https://doi.org/10.1016/j.cap.2011.01.034

[20] Li B, Blendell JE, & Bowman KJ. (2011). Temperature-dependent poling behavior of lead-free BZT-BCT piezoelectrics. Journal of the American Ceramic Society, 94(10), 3192-3194. https://doi.org/10.1111/j.1551-2916.2011.04758.x

[21] Wang W, He JY, Sun QF, Yang RY, Cui FJ, & Ren X. (2019). Enhanced Piezoelectric Properties and Temperature Stability of 0.5 BZT-0.5 BCT Ceramic Induced by Using Three-Step Synthesizing Method. ECS Journal of Solid State Science and Technology, 8(9), N134. https://doi.org/10.1149/2.0191909jss

[22] Tuan DA, Tung V, Chuong TV, Tinh NT, & Huong NTM. (2015). Structure, microstructure and dielectric properties of lead-free BCT-xBZT ceramics near the morphotropic phase boundary.

[23] Tan Y, Zhang J, Wu Y, Wang C, Koval V, Shi B, & Yan H. (2015). Unfolding grain size effects in barium titanate ferroelectric ceramics. Scientific reports, 5(1), 1-9. https://doi.org/10.1038/srep09953

[24] Xue D, Zhou Y, Bao H, Gao J, Zhou C, & Ren X. (2011). Large piezoelectric effect in Pb-free Ba (Ti, Sn) O3-x (Ba, Ca) TiO3 ceramics. Applied Physics Letters, 99(12), 122901. https://doi.org/10.1063/1.3640214

[25] Liu W, & Ren X. (2009). Large piezoelectric effect in Pb-free ceramics. Physical review letters, 103(25), 257602. https://doi.org/10.1103/PhysRevLett.103.257602

[26] Dobal PS, Dixit A, Katiyar RS, Yu Z, Guo R, & Bhalla A. S. (2001). Micro-Raman scattering and dielectric investigations of phase transition behavior in the BaTiO 3-BaZrO 3 system. Journal of Applied Physics, 89(12), 8085-8091. https://doi.org/10.1063/1.1369399

[27] Fu J, Zuo R, Wu SC, Jiang JZ, Li L, Yang TY, & Li L. (2012). Electric field induced intermediate phase and polarization rotation path in alkaline niobate based piezoceramics close to the rhombohedral and tetragonal phase boundary. Applied Physics Letters, 100(12), 122902. https://doi.org/10.1063/1.3696071

[28] Li W, Xu Z, Chu R, Fu P, & Zang G. (2010). Polymorphic phase transition and piezoelectric properties of (Ba1− xCax)(Ti0. 9Zr0. 1) O3 lead-free ceramics. Physica B: Condensed Matter, 405(21), 4513-4516. https://doi.org/10.1016/j.physb.2010.08.028

[29] Azároff LV. (1980). X-ray diffraction by liquid crystals. Molecular Crystals and Liquid Crystals, 60(1-2), 73-97. https://doi.org/10.1080/00268948008072426

[30] Kumar N, Sidhu GK, & Kumar R. (2019). Correlation of synthesis parameters to the phase segregation and lattice strain in tungsten oxide nanoparticles. Materials Research Express, 6(7), 075019. https://doi.org/10.1088/2053-1591/ab12a5

[31] Williamson GK, & Hall WH. (1953). X-ray line broadening from filed aluminium and wolfram. Acta metallurgica, 1(1), 22-31. https://doi.org/10.1016/0001-6160(53)90006-6

[32] Kumar P, Prakash C, Thakur OP, Chatterjee R, & Goel TC. (2006). Dielectric, ferroelectric and pyroelectric properties of PMNT ceramics. Physica B: Condensed Matter, 371(2), 313-316. https://doi.org/10.1016/j.physb.2005.10.107

[33] Bokov AA, & Ye ZG. (2020). Recent progress in relaxor ferroelectrics with perovskite structure. Progress in Advanced Dielectrics, 105-164. https://doi.org/10.1142/9789811210433_0003

[34] Liu Y, Pu Y, & Sun Z. (2014). Enhanced relaxor ferroelectric behavior of BCZT lead-free ceramics prepared by hydrothermal method. Materials Letters, 137, 128-131. https://doi.org/10.1016/j.matlet.2014.08.138

[35] Wang Z, Wang J, Chao X, Wei L, Yang B, Wang D, & Yang Z. (2016). Synthesis, structure, dielectric, piezoelectric, and energy storage performance of (Ba 0.85 Ca 0.15)(Ti 0.9 Zr 0.1) O 3 ceramics prepared by different methods. Journal of Materials Science: Materials in Electronics, 27(5), 5047-5058. https://doi.org/10.1007/s10854-016-4392-x

[36] Praveen JP, Karthik T, James AR, Chandrakala E, Asthana S, & Das D. (2015). Effect of poling process on piezoelectric properties of sol-gel derived BZT-BCT ceramics. Journal of the European Ceramic Society, 35(6), 1785-1798. https://doi.org/10.1016/j.jeurceramsoc.2014.12.010

[37] Badapanda T, Sarangi S, Behera B, & Anwar S. (2014). Structural and impedance spectroscopy study of Samarium modified Barium Zirconium Titanate ceramic prepared by mechanochemical route. Current Applied Physics, 14(9), 1192-1200. https://doi.org/10.1016/j.cap.2014.06.007

[38] Dash U, Sahoo S, Chaudhuri P, Parashar SKS, & Parashar K. (2014). Electrical properties of bulk and nano Li 2 TiO 3 ceramics: A comparative study. Journal of Advanced Ceramics, 3(2), 89-97. https://doi.org/10.1007/s40145-014-0094-0

[39] Tiwari B, & Choudhary RNP. (2010). Study of impedance parameters of cerium modified lead zirconate titanate ceramics. IEEE Transactions on Dielectrics and Electrical Insulation, 17(1), 5-17. https://doi.org/10.1109/TDEI.2010.5411996

[40] Tiwari B, & Choudhary RNP. (2010). Frequency-temperature response of Pb (Zr0. 65− xCexTi0. 35) O3 ferroelectric ceramics: impedance spectroscopic studies. Journal of alloys and compounds, 493(1-2), 1-10. https://doi.org/10.1016/j.jallcom.2009.11.120

[41] Singh H, Kumar A, & Yadav KL. (2011). Structural, dielectric, magnetic, magnetodielectric and impedance spectroscopic studies of multiferroic BiFeO3-BaTiO3 ceramics. Materials Science and Engineering: B, 176(7), 540-547. https://doi.org/10.1016/j.mseb.2011.01.010

[42] Wang X, Liang P, Chao X, & Yang Z. (2015). Dielectric properties and impedance spectroscopy of MnCO3-modified (Ba0. 85Ca0. 15)(Zr0. 1Ti0. 9) O3 lead-free ceramics. Journal of the American Ceramic Society, 98(5), 1506-1514. https://doi.org/10.1111/jace.13481

[43] Chen X, Wang Y, Chen J, Zhou H, Fang L, & Liu L. (2013). Dielectric Properties and Impedance Analysis of K 0.5 Na 0.5 NbO 3-Ba 2 NaNb 5 O 15 Ceramics with Good Dielectric Temperature Stability. Journal of the American Ceramic Society, 96(11), 3489-3493. https://doi.org/10.1111/jace.12514

[44] Li YM, Liao RH, Jiang XP, & Zhang YP. (2009). Impedance spectroscopy and dielectric properties of Na0. 5Bi0. 5TiO3-K0. 5Bi0. 5TiO3 ceramics. Journal of Alloys and

Compounds, 484(1-2), 961-965. https://doi.org/10.1016/j.jallcom.2009.05.087

[45] Ranjan R, Kumar R, Behera B, & Choudhary RNP. (2009). Structural and impedance spectroscopic studies of samarium modified lead zirconate titanate ceramics. Physica B: Condensed Matter, 404(20), 3709-3716. https://doi.org/10.1016/j.physb.2009.06.113

[46] Biswal MR, Nanda J, Mishra NC, Anwar S, & Mishra A. (2014). Dielectric and impedance spectroscopic studies of multiferroic BiFe1-xNixO3. Adv. Mater. Lett., 5(9), 531-537. https://doi.org/10.5185/amlett.2014.4566

[47] Dutta S, Choudhary RNP, & Sinha PK. (2007). Impedance spectroscopy studies on Fe3+ ion modified PLZT ceramics. Ceramics international, 33(1), 13-20. https://doi.org/10.1016/j.ceramint.2005.07.010

[48] Sen S, Choudhary RNP, Tarafdar A, & Pramanik P. (2006). Impedance spectroscopy study of strontium modified lead zirconate titanate ceramics. Journal of applied physics, 99(12), 124114. https://doi.org/10.1063/1.2206850

[49] Macdonald JR. (1987). Impedance spectroscopy (Vol. 346). Wiley, New York.

[50] Das PS, Chakraborty PK, Behera B, & Choudhary RNP. (2007). Electrical properties of Li2BiV5O15 ceramics. Physica B: Condensed Matter, 395(1-2), 98-103. https://doi.org/10.1016/j.physb.2007.02.065

[51] Jha AK. (2013). Electrical characterization of zirconium substituted barium titanate using complex impedance spectroscopy. Bulletin of Materials Science, 36(1), 135-141. https://doi.org/10.1007/s12034-013-0420-0

[52] Behera AK, Mohanty NK, Satpathy SK, Behera B, & Nayak P. (2014). Investigation of complex impedance and modulus properties of Nd doped 0.5 BiFeO 3-0.5 PbTiO 3 multiferroic composites. Central European Journal of Physics, 12(12), 851-861. https://doi.org/10.2478/s11534-014-0523-2

[53] Shukla A, & Choudhary RNP. (2011). High-temperature impedance and modulus spectroscopy characterization of La3+/Mn4+ modified PbTiO3 nanoceramics. Physica B: Condensed Matter, 406(13), 2492-2500. https://doi.org/10.1016/j.physb.2011.03.030

[54] Ortega N, Kumar A, Bhattacharya P, Majumder SB, & Katiyar RS. (2008). Impedance spectroscopy of multiferroic Pb Zr x Ti 1− x O 3⁄Co Fe 2 O 4 layered thin films. Physical review B, 77(1), 014111. https://doi.org/10.1103/PhysRevB.77.014111

[55] Bergman, R. (2000). General susceptibility functions for relaxations in disordered systems. Journal of Applied Physics, 88(3), 1356-1365. https://doi.org/10.1063/1.373824

[56] Gerhardt R. (1994). Impedance and dielectric spectroscopy revisited: distinguishing localized relaxation from long-range conductivity. Journal of Physics and Chemistry of Solids, 55(12), 1491-1506. https://doi.org/10.1016/0022-3697(94)90575-4

Received on 14-02-2021 Accepted on 25-01-2022 Published on 03-03-2022

DOI: https://doi.org/10.31875/2409-9848.2022.09.4